SSR Journal of Multidisciplinary (SSRJM)



Volume 2, Issue 9, 2025

Homepage: https://ssrpublisher.com/ssrjm/
Email: office.ssrpublisher@gmail.com



ISSN: 3049-1304

Boundary Layer Analysis of Non-Darcian Casson Fluid Flow Conveying Hybrid Nanoparticles with Unequal Diffusivities over a Surface with Variable Thickness

Emmanuel Omokhuale¹, Segun Raphael Adebayo², Kazeem Adekunle Okunlola², Olubaji Simeon Olawumi³, Kamorudeen Abiodun Adeoye², Adebayo Stephen Oladoja⁴, Tosin Oreyeni²

Received: 20.09.2025 | Accepted: 17.10.2025 | Published: 19.10.2025

*Corresponding Author: Tosin Oreyeni

DOI: 10.5281/zenodo.17392286

Abstract Review Article

This study incorporates trihybrid nanoparticles into Casson fluid with stratification, non-Darcian term, radiation and quartic autocatalytic chemical reaction effects over an upper surface of paraboloid of revolution. The impact of thermal stratification is examined to gain insight into its effect on boundary layer structure and energy distribution. The flow phenomenon is described by governing equations that are converted and parameterized using suitable similarity variables. The nonlinear ordinary differential equations obtained are subsequently resolved using the MATLAB package (bvp4c). Throughout the flow analysis, specific flow parameters are scrutinized, revealing their substantial impact on different distributions. It was noticed that the homogeneous bulk fluid is enhanced with the growing upshot of the Grashof number. Furthermore, an augmentation in the Brownian motion parameter leads to a higher effective thermal conductivity of the nanofluid.

Keywords: Trihybrid nanofluid, Casson fluid, Quartic autocatalytic chemical Reaction, Darcy-Forchheimer, Variable thickness.

Copyright © 2025 The Author(s). This is an open-access article distributed under the terms of the Creative Commons Attribution-NonCommercial 4.0 International License (CC BY-NC 4.0).

1. Introduction

Solar energy which is the most environmentally-friendly form of renewable energy harnessed directly from the sun is known to possess the capability to generate heat, initiate chemical reactions, and produce electricity. The energy of the sun can be harnessed through various methods and employed for electricity production. Photovoltaic systems consist of solar panels made up of photovoltaic cells constructed from semiconductor materials which operate on the principles of the photoelectric effect. As sunlight interacts with photovoltaic cells, electrons are excited, resulting in the generation of electricity. The electrical potential

produced by the photovoltaic effect is then captured and channeled through an inverter, transforms the direct current (DC) generated by the cells into alternating current (AC) suitable for immediate utilization [2]. Owing to the advancement of the renewable energy system, many authors have contributed immensely to this field. Thapa *et al.*[3] focused on the potentiality and constraints in solar photovoltaic cells to produce electricity. They recorded production of electricity is being affected by factors such as energy policy, financial factors, social and cultural factors. Elomari et al. [4] presented how renewable energy sources served to ameliorate the technical and economic integration into power networks. De Brito et al.



¹Department of Mathematical Sciences, Federal University Gusau, Nigeria

²Department of Mathematical Sciences, Osun State University, Osogbo, Nigeria

³Department of Software Engineering, Westland University, Iwo, Nigeria

⁴Department of Mathematics, Modibbo Adama University, Yola, Nigeria

[5] considered a number of trends in the area of photovoltaic energy conversion highlighting innovations such as the creation of thinner and more efficient solar cells and the usage of silicon carbide devices in PV inverters.

Nanofluids are comprised of nanoparticles from (1-100nm)suspended ranging conventional fluids. These fluids exhibit low thermal conductivity but hold great potential in applications relating to heat transfer owing to their enhanced thermal properties. Generally, it is expected that nanofluids will demonstrate enhanced thermal performance in comparison to conventional fluids, as nanoparticles boast high thermal conductivity. It has been extensively analysed by several researchers that the utilization of nanofluids in various applications leads to a conspicuous enhancement in heat transfer efficiency when compared to traditional fluids. Shah [6] carried out an examination on the behaviour of micropolar fluid containing nanoparticles and microorganisms in stagnation point flow.

Thermal analysis of ternary hybrid nanofluid passing through a permeable slipped surface was explored by Ramesh et al.[7]. morphological influences of hydromagnetic flow of micropolar fluid with nanoparticles between two parallel plates were discussed by Rauf et al. [8]. Ramesh et al.[9] presented magnetic field impact on radiative heat transfer hybrid nanofluid flow over an exponentially stretching surface. Koriko et al. [10] presented the active and passive cases of a thixotropic nanofluid flow over a vertical surface. Their findings indicated that Brownian motion plays a role in the heating of particle molecules, enhancing thermal conductivity and leading to an increase in fluid temperature. In a study conducted separately, Shah et al. [11] explored the implication of Brownian motion on Casson fluid flow over a non-uniform surface. The significance radiation on boundary layer analysis of Boger fluid containing nanoparticles through the use of finite element analysis was conducted by Raza et al. [12]. Babu et al [13] investigated the squeezed flow of water-based fluid with nanoparticles over a magnetized sensor surface. The addition of three different nanoparticles into base have been termed as trihybrid. The incorporation of nanoparticles improves specific fluid properties, including thermal conductivity, stability, and heat transfer capabilities. The improved thermal characteristics of nanofluids make them suitable for use in various fields. Asogwa et al.14] presented thermal diffusion impact on the hydromagnetic flow a non-Newtonian fluid conveying nanoparticles over a stretched Riga surface. Aluminium Oxide $(Al_2 O_3)$ is a form of nanoparticles that display unique characteristics and have the potential for various applications across multiple industries. Rasool et al.[15] considered numerical techniques Electrohydromagnetic nanofluid flow over a convectively heated surface. Boundary layer flow of Carreau-Yasuda tri-hybrid nanofluid flow over a convectively heated surface near a stagnation point was presented Rauf et al.[16]. Yu et al.[17] investigated heat transfer analysis through viscous ternary hybrid nanofluid over a stretching/shrinking thin needle. Kumar et al. [18] proposed a sophisticated deep learning approach for predicting heat transfer flow of fluid conveying nanoparticles. Ramasekhar et al.[19] studied boundary layer flow of Casson fluid conveying hybrid nanoparticles with heat source/since implication. Kumar et al. [20] delved into the optimisation of a thermal management system using machine learning and nanofluids for precise heat transfer analysis. Yaseen et al. [21] investigated the impact of thermal radiation on bioconvective flow with three distinct nanoparticles across various Their findings indicate that the geometries. temperature of a ternary hybrid nanofluid rises in response to increased radiation and variations in heat source/sink parameters. Vinodkujar et al. [22] explored mixed convetion flow of Ree-Eyring fluid with tinyparticles and gyrotactic Yahya et al.[23] presented microorganisms. modified Buongiorno model for hydromagnetic micropolar and Casson fluid flow with nonlinear thermal radiation impact. Ramasekhar and Shah [24] discussed Casson fluid flow with hybrid nanoparticles through a stretching surface with thermal radiation effect. Bioconvective Riga wedge flow of tangent hyperbolic nanofluids with activiation energy was studied by Li et al. [25].

The process of stratification is essential in



various technologies such as thermal energy storage systems and solar water heaters. Solar water heaters rely on stratification to ensure that hot water remains at the top of the storage tank, while cooler water settles at the bottom. addition, thermal energy storage system operates on the concept of stratification to store and release heat energy for different purposes including concentrated solar power plants and district heating systems, as highlighted by Popoola et al. [26]. Tamilzharasan et al. [27] examined stratification effect on convective flow of Williamson fluid within a porous medium. Jagan et al. [28] conducted an analysis on the influence stratification on magnetohydrodynamic fluid flow over stretching cylinder. Rehman et al. [29] examined the behaviour of a thermally stratified Eyring-Powel fluid with a phase change phenomenon. Oreyeni et al. [30] emphasized the impact stratification and heat generation on fluid with microstructures. It was indicated that heightened stratification resulted in a decrease in temperature difference between the wall and outside the boundary layer. Olanrewaju et al. [31] investigated implication of doubly stratified Upper-Convected Maxwell fluid with variable Khan et al. [32] presented characteristics. stratification phenomena on a Sutterby nanofluid. Guedri et al. [33] investigated utilization of spiral fins to improve latent heat tube-shell storage system. Dogonchi et al. [34] discussed heat transfer effect utilizing phase change materials encapsulated at the nano scale. Priyadharshini et al. [35] presented hydromagnetic fluid flow with Gradient descent machine learning regression.

Two commonly utilised forms of catalysis in industrial both settings and everyday applications include homogeneous heterogeneous catalytic chemical reactions. Homogeneous catalysis involves the catalyst and reactants being in the same phase and evenly dispersed throughout the reaction mixture. This type of catalysis is frequently employed in the production of polymers, pharmaceuticals, and specialty chemicals. In contrast, heterogeneous catalytic reactions involve the catalyst and reactants existing in separate phases. For example, the reactants may be in a gaseous or liquid state while the catalyst remains solid. Heterogeneous catalysis is widely used in a wide range of industrial processes, including fuel and chemical production, petroleum refining, and environmental applications like exhaust gas pollution removal. Both homogeneous and heterogeneous catalytic chemical reactions are essential to many aspects of daily life and industry. Research has been conducted on flow homogeneous-heterogeneous owing to its importance in the industry. A recent study by Sravanthi et al. [36] analysed the behaviour of magnetite-water nanofluid under the influence of both homogeneous and heterogeneous effects. Alzahrani et al. [37] investigated the impacts of thermosolutal Marangoni convection on chemically reacting Oldroyd-B fluid. Sarojamma et al. [38] explored the heat and mass flux effect of micropolar fluid with autocatalytic chemical reaction involving micropolar fluid. Their findings indicated that the presence of microstructures leads to a decrease in the concentration of homogenous bulk fluid, while increasing the concentration of catalyst at the surface. Animasaun et al. [39] examined the development of a boundary layer on a surface subjected to Eyring-Powell liquid of differing thicknesses and consistent diffusivity. Hayat et al. [40] investigated the impacts of uniform and non-uniform reactions on the flow of nanofluid over a surface with irregular thickness. Zhao et al. [41] utilised Buongiorno's model to analyse the flow properties of nanofluid in the occurrence of both uniform and nonuniform reactions.

Drawing inspiration from the studies mentioned above, we aim to investigate the efficacy of three distinct nanoparticles TiO_2, ZnO, Al_2O_3 in relation to photovoltaic systems featuring stratifications and quartic autocatalytic chemical reactions. It is widely acknowledged that the incorporation of nanoparticles has the potential to increase the temperature of solar panel cells, thereby enhancing both the electrical and thermal efficiency of the cells.

2. Mathematical formulation

In this communication the dynamics of Casson ternary hybrid nanofluid with stratification and homogeneous-heterogeneous



chemical reaction across a nonlinear surface is presented. TiO_2, ZnO, Al_2O_3 Have been incorporated into the fluid model owing to their high efficiency on the solar panel cells. The Casson fluid is engrossed with engine oil base fluid. A homogeneous-heterogeneous chemical reaction between the concentrated catalyst on the wall and the reactant (bulk fluid) is assumed. The expansion in the sheet is nonlinear which is moving with a nonlinear velocity $U_w = ax^m$, where a is constant value x is the distance away from the slit while m is the nonlinearity index of

the stretching sheet. λ and r represents the chemical species homogeneous bulk fluid A (Casson fluid) and heterogeneous of catalyst B at the wall concentrations, respectively. However, the u and v are the velocities along x, y – directions, temperature is T(x, y), concentrations of reactant A and reactant B are $\lambda(x, y)$ and r(x, y) see [42]-[44].

Following Gandhi et al. [45], Popoola et al. [46] the rheological expression of an isotropic and incompressible flow of a Casson fluid can be written as

$$\tau_{ij} = \begin{cases} 2\left(\mu_b + \frac{p_y}{\sqrt{2\pi}}\right)e_{ij}, & \pi > \pi_c \\ 2\left(\mu_b + \frac{p_y}{\sqrt{2\pi}c}\right)e_{ij}, & \pi < \pi_c \end{cases}$$
(1)

where p_y is the yield stress of fluid, μ_b is the plastic dynamic viscosity of the non-Newtonian fluid, the (i,j)th component of the deformation rate is e_{ij} , the product of e_{ij} with itself is $\pi = e_{ij}e_{ji}$ and critical value of this product based on the non-Newtonian model is π_c , the product of the component of deformation rate with itself is π .

Given the above-mentioned assumptions and the equations governing the fluid flow appropriate for examining a ternary hybrid Casson nanofluid with stratification and homogeneous-heterogeneous chemical reaction on the upper horizontal surface of a paraboloid of revolution aligns with the formulations of [22], [30], [38], [39], [42], [43], [44] is presented as

Continuity Equation

$$\frac{\partial u}{\partial x} + \frac{\partial v}{\partial y} = 0,\tag{2}$$

Momentum Equation

$$u\frac{\partial u}{\partial x} + v\frac{\partial u}{\partial y} = \left(1 + \frac{1}{\beta}\right)\frac{\mu_{thnf}}{\rho t_{hnf}}\frac{\partial}{\partial y}\left(\frac{\partial u}{\partial y}\right) + g\beta_t \frac{(m+1)}{2}(T - T_\infty) - \frac{\mu_{thnf}}{\rho_{thnf}}\left(1 + \frac{1}{\beta}\right)\frac{1}{k}u - \frac{b^*}{k}u^2, \tag{3}$$

Energy Equation

$$u\frac{\partial T}{\partial x} + v\frac{\partial T}{\partial y} = \frac{k_{thnf}}{\left(\rho C_{p}\right)_{thnf}} \frac{\partial}{\partial y} \left(\frac{\partial T}{\partial y}\right) + \frac{16}{3} \frac{1}{\left(\rho C_{p}\right)_{thnf}} \left(\frac{\sigma^{*}T^{3}}{k^{*}} \frac{\partial}{\partial y} \left(\frac{\partial T}{\partial y}\right)\right) + \tau \left(D_{B} \left(\frac{\partial T}{\partial y} \frac{\partial C}{\partial y}\right) + \frac{D_{T}}{T_{\infty}} \left(\frac{\partial T}{\partial y}\right)^{2}\right), (4)$$

Homogeneous species Equation

$$u\frac{\partial\lambda}{\partial x} + v\frac{\partial\lambda}{\partial y} = D_A \frac{\partial^2\lambda}{\partial y^2} - \frac{D_T}{T_\infty} \frac{\partial}{\partial y} \left(\frac{\partial T}{\partial y}\right) - k_h \lambda r^3, \tag{5}$$

Heterogeneous specie equation

$$u\frac{\partial r}{\partial x} + v\frac{\partial r}{\partial y} = D_B \frac{\partial^2 r}{\partial y^2} + \frac{D_T}{T_\infty} \frac{\partial}{\partial y} \left(\frac{\partial T}{\partial y}\right) + k_h \lambda r^3 \tag{6}$$



Subjected to the following boundary conditions

$$u = ax^{m}, v = 0, T = T_{w}, \frac{1}{\lambda} \frac{\partial \lambda}{\partial y} = \frac{K_{s}}{D_{A}}, \frac{1}{-\lambda} \frac{\partial r}{\partial y} = \frac{K_{s}}{D_{B}} \quad \text{at } y = A(x+b)^{\frac{1-m}{2}},$$

$$u \to 0, T \to T_{\infty}, \quad \lambda \to \delta, \quad r \to 0, \quad \text{as } y \to \infty$$

$$(7)$$

Where β is the Casson fluid parameter, ρC_p is the heat capacity Q_o is the heat generation/absorption, B_o is the magnetic field strength, T is the fluid temperature, κ is thermal conductivity, ρ_f is the fluid density κ is thermal conductivity and σ_f is the fluid electrical conductivity. Fig 1 shows the schematic display of the model

The similarity transformations can be expressed as

$$u = \frac{\partial \psi}{\partial y} = U_0(x+b)^m \frac{df}{d\aleph},$$

$$v = -\frac{\partial \psi}{\partial x} = -\left[U_0(x+b)^{m-1}y^{\frac{m-1}{2}}\frac{df}{d\aleph} + \frac{m+1}{2}\left(\frac{2\vartheta U_0}{m+1}\right)^{\frac{1}{2}}(x+b)^{\frac{m-1}{2}}f(\aleph)\right],$$

$$\aleph = y\left(\frac{U_0(m+1)}{2\vartheta}\right)^{\frac{1}{2}}(x+b)^{\frac{m-1}{2}}, \quad \psi = \left(\frac{2\vartheta U_0}{m+1}\right)^{\frac{1}{2}}(x+b)^{\frac{m+1}{2}}f(\aleph),$$

$$\theta(\aleph) = \frac{T-T_\infty}{T_W-T_0}, \quad \frac{\lambda}{\delta} = q(\aleph), \quad \frac{r}{\delta} = s(\aleph)$$

$$(8)$$

It is to be noted that stratification at the wall (T_w) and at the free stream (T_∞) are expressed as

$$T_w - T_0 = m_1(x+b)^{\frac{1-m}{2}}, \quad T_\infty - T_0 = m_2(x+b)^{\frac{1-m}{2}},$$
 (9)

Where T_0 depicts the reference temperature.

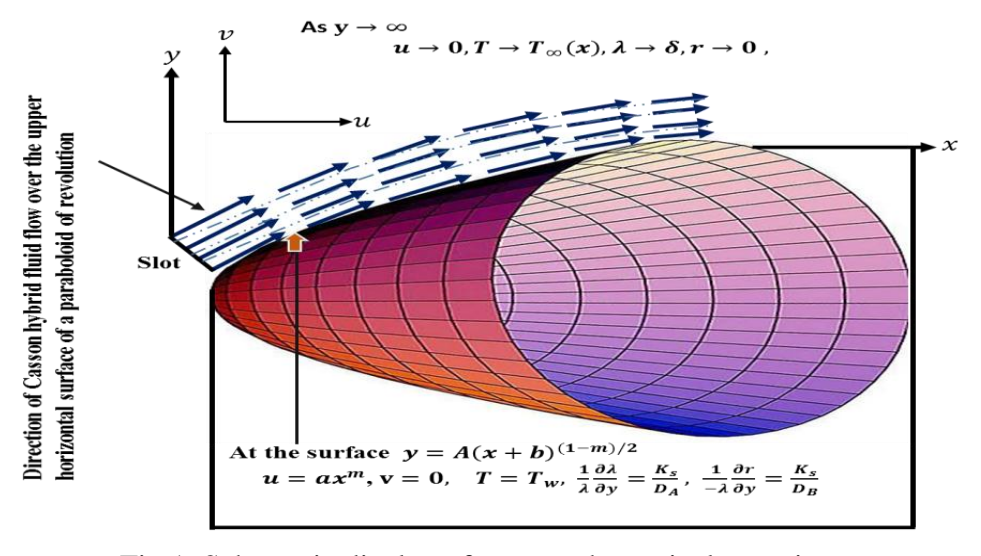


Fig 1. Schematic display of present theoretical experiment

Thermophysical characteristics of ternary hybrid nanofluid [20]

$$\begin{split} \frac{\mu_{thnf}}{\mu_f} &= \frac{1}{(1-\phi_1)^{2.5}(1-\phi_2)^{2.5}(1-\phi_1)^{2.5}} \, . \\ \frac{\rho_{thnf}}{\rho_f} &= (1-\phi_1) \left[(1-\phi_2) \left\{ (1-\phi_3) + \phi_3 \frac{\rho_3}{\rho_f} \right\} \right. + \phi_2 \frac{\rho_2}{\rho_f} \right] + \phi_1 \frac{\rho_1}{\rho_f}, \\ \frac{k_{thnf}}{k_{hnf}} &= \left(\frac{k_1 + 2k_{hnf} - 2\phi_1(k_{hnf} - k_1)}{k_1 + 2k_{hnf} + \phi_1(k_{hnf} - k_1)} \right), \\ \frac{k_{hnf}}{k_{nf}} &= \left(\frac{k_2 + 2k_{nf} - 2\phi_2(k_{nf} - k_2)}{k_2 + 2k_{nf} + \phi_2(k_{nf} - k_2)} \right), \\ \frac{k_{nf}}{k_f} &= \left(\frac{k_3 + 2k_f - 2\phi_3(k_f - k_3)}{k_3 + 2k_f + \phi_3(k_f - k_3)} \right), \\ \frac{(\rho c p)_{thnf}}{(\rho c p)_f} &= (1 - \phi_1) \left[(1 - \phi_2) \left\{ (1 - \phi_3) + \phi_3 \frac{(\rho c p)_3}{(\rho c p)_f} \right\} \right. + \phi_2 \frac{(\rho c p)_2}{(\rho c p)_f} \right] + \phi_1 \frac{(\rho c p)_1}{(\rho c p)_f} \end{split}$$

Experimental values of nanoparticles and base fluid are depicted in Table 1 following the studies of [20, 22].

Table 1: Thermo-physical properties of nanomaterials

Thermo-physical Properties	$\rho(kgm^{-3})$	$C_p(Jkg^{-1}K^{-1})$	$K(Wm^{-1}K^{-1})$	$\sigma\left(\frac{s}{m}\right)$
Engine Oil	884	1910	0.144	
Titanium oxide (TiO_2) (s1)	4250	686.2	8.9538	$10^{-9} - 10^{11}$
Zinc Oxide (ZnO) (s2)	5600	495.2	13	
Aluminum oxide $(Al_2 O_3)$ (s3)	3970	765	40	3.5×10^6

Using the similarity transformations, the governing equations (2)-(6) with boundary condition (7) can be expressed as

$$\left(1 + \frac{1}{\beta}\right) \frac{d^{3} f}{d\aleph^{3}} + (1 - \phi_{1})^{2.5} (1 - \phi_{2})^{2.5} (1 - \phi_{3})^{2.5} (1 - \phi_{1})
\left[(1 - \phi_{2})\left\{(1 - \phi_{3}) + \phi_{3} \frac{\rho_{3}}{\rho_{f}}\right\} + \phi_{2} \frac{\rho_{2}}{\rho_{f}}\right] \phi_{1} \frac{\rho_{1}}{\rho_{f}} \left(f \frac{d^{2} f}{d\aleph^{2}} - \frac{2m}{m+1} \frac{df}{d\aleph} \frac{df}{d\aleph} + G_{r}\theta\right)
- \frac{2}{m+1} \left(1 + \frac{1}{\beta}\right) P_{s} \frac{df}{d\aleph} - \frac{2}{m+1} F_{s} D_{a}^{-1} \frac{df}{d\eta} \frac{df}{d\eta} = 0,$$
(10)

$$\frac{k_{thnf}}{k_f} \left[1 + \frac{4R_a}{3} \right] \frac{d^2\theta}{d\aleph^2} + (1 - \phi_1) \left[(1 - \phi_2) \left\{ (1 - \phi_3) + \phi_3 \frac{(\rho c p)_3}{(\rho c p)_f} \right\} \right. + \phi_2 \frac{(\rho c p)_2}{(\rho c p)_f} \right]$$

$$+ \phi_1 \frac{(\rho c p)_1}{(\rho c p)_f} \left(P_r f \frac{d\theta}{d\aleph} - P_r \frac{2}{m+1} (\theta + S_t) \frac{df}{d\aleph} + P_r N_b \frac{d\theta}{d\aleph} \frac{d\phi}{d\aleph} + P_r N_t \frac{d\theta}{d\aleph} \frac{d\theta}{d\aleph} + \frac{2}{m+1} \zeta P_r E x p^{-n\aleph} \right) = 0,$$

$$(11)$$

$$\frac{d^2q}{d\aleph^2} + S_{cA}f \frac{dq}{d\aleph} - \frac{N_t}{N_h} \frac{d^2\theta}{d\aleph^2} - \frac{2}{m+1} S_{cA}\mathcal{R}q(\aleph) s^3(\aleph) = 0, \tag{12}$$

$$\gamma \frac{d^2s}{d\aleph^2} + S_{cB} f \frac{ds}{d\aleph} - \frac{N_t}{N_h} \frac{d^2\theta}{d\aleph^2} + \frac{2}{m+1} S_{cB} \mathcal{R} q(\aleph) s^3(\aleph) = 0, \qquad (13)$$



The Boundary Conditions become

$$(\aleph) = 0, \frac{df}{d\aleph} = 1, \ \theta(\aleph) = 1 - S_t, \frac{dq}{d\aleph} = \mathcal{J}q(\aleph), \frac{ds}{d\aleph} = -\mathcal{J}q(\aleph), \quad at \ \aleph = 0$$

$$\gamma \frac{df}{d\aleph} \to 0, \theta(\aleph) \to 0, q(\aleph) \to 1, s(\aleph) \to 0 \quad as \ \aleph \to \infty$$

$$(14)$$

Where Newtonian parameter is β , velocity index is m, Porosity parameter $Ps = \frac{\vartheta}{kc(x+b)^{m-1}}$, Grashof number $Gr = \frac{g\beta(T_W - T_0)}{c^2(x+b)^{2m-1}}$, Solar thermal radiation parameter $Ra = \frac{4\sigma^*T_0^3}{k\ k^*}$, Prandtl number $Pr = \frac{\vartheta}{\alpha}$, Spacedependent internal heat source parameter $\zeta = \frac{Q_0}{\rho C_p c(x+b)^{m-1}}$, thermal stratification parameter $St = \frac{m_2}{m_1}$, Brownian motion parameter $Nb = \frac{\tau\ D_A\delta}{\alpha}$, Thermophoresis parameter $Nt = \frac{\tau(T_W - T_0)}{\alpha} \frac{D_T}{T_\infty}$, Schmidth number for specie A $Sc_A = \frac{\vartheta}{D_A}$, Schmidth number for specie B $Sc_B = \frac{\vartheta}{D_B}$, homogeneous reaction parameter $\mathcal{R} = \frac{\vartheta}{D_B}$

$$\frac{k_h \delta^3}{c(x+b)^{m-1}}, \text{ ratio of diffusion constants } \gamma = \frac{D_B}{D_A}, \text{ and strength of heterogeneous parameter } \mathcal{J} = \frac{\left(\frac{c\ (m+1)}{2\vartheta b_f}\right)^{-\frac{1}{2}}}{D_A(x+b)^{\frac{m-1}{2}}}.$$

The wall friction coefficient C_{fx} , Local Nusselt number Nu_x

$$C_{fx} = \frac{\tau_w}{\rho_f \sqrt{\frac{m+1}{2}(U_w)^2}},$$

$$Nu_x = \frac{(x+b)q_w}{\kappa_f (T_w - T_0) \sqrt{\frac{m+1}{2}}},$$
(15)

Where,

$$\tau_{w} = \mu_{thnf} \left(1 + \frac{1}{\beta} \frac{\partial u}{\partial y} \Big|_{y_{w}}, \right)$$

$$q_{w} = -k_{thnf} \frac{\partial T}{\partial y} \Big|_{y_{w}},$$

$$(16)$$

Substituting the expression for τ_w into C_{fx} and q_w into Nu_x then,

$$C_{fx} = \left[\frac{\mu_f \left(1 + \frac{1}{\beta} \right)}{\rho_f \sqrt{\frac{m+1}{2} (U_w)^2}} \right] \frac{\partial u}{\partial y} \Big|_{y = A(x+b)^{\frac{1-m}{2}}},$$

$$Nu_x = -\left[\frac{(x+b)q_w}{(T_w - T_0)\sqrt{\frac{m+1}{2}}} \right] \frac{\partial T}{\partial y} \Big|_{y = A(x+b)^{\frac{1-m}{2}}}$$

$$(17)$$

The shear stress (skin friction) between Casson fluid and upper surface of horizontal paraboloid of revolution is τ_w and q_w is the heat flux from the wall. Utilizing the eqns. (9) we obtain

$$Re_{x}^{\frac{1}{2}}C_{fx} = \frac{\left(1+\frac{1}{\beta}\right)}{(1-\phi_{1})^{2.5}(1-\phi_{2})^{2.5}(1-\phi_{1})^{2.5}}f''(0),$$

$$Nu_{x}Re_{x}^{-\frac{1}{2}} = -\left(\frac{k_{thnf}}{k_{f}} + \frac{4}{3}R_{a}\right)\theta'(0)$$
(18)

Where Local Reynolds number is indicated and defined as $Re_x = \frac{U_w(x+b)}{\vartheta_f}$.

3. Numerical Solution

BVP4C is a numerical approach that applies a collocation methodology to address boundary



value problems associated with Ordinary Differential Equations. This technique involves the discretization of the ODEs through a finite difference scheme, effectively breaking down the domain into smaller subintervals. Within this framework the resultant system of nonlinear equations is resolved by means of the Newton iteration technique. Equations (10) - (14) are then transformed into a first-order differential equation. Let

$$f = y_1, f' = y_2, f'' = y_3, f''' = y_3',$$
 (19)

$$\left(1 + \frac{1}{\beta}\right) y_3' = (1 - \phi_1)^{2.5} (1 - \phi_2)^{2.5} (1 - \phi_3)^{2.5}$$

$$* (1 - \phi_1) \left[(1 - \phi_2) \left\{ (1 - \phi_3) + \phi_3 \frac{\rho_3}{\rho_f} \right\} + \phi_2 \frac{\rho_2}{\rho_f} \right]$$
(20)

$$+\phi_1 \frac{\rho_1}{\rho_f} \left(\frac{2m}{m+1} y_2 y_2 - y_1 y_3 - G_r y_4 \right) + \left(1 + \frac{1}{\beta} \right) \frac{2}{m+1} P_s y_2,$$

$$\theta = y_4, \ \theta' = y_5, \ \theta'' = y_5'$$
 (21)

$$\frac{\frac{k_{thnf}}{k_{f}}}{(1-\phi_{1})\left[(1-\phi_{2})\left\{(1-\phi_{3})+\phi_{3}\frac{(\rho c p)_{3}}{(\rho c p)_{f}}\right\}+\phi_{2}\frac{(\rho c p)_{2}}{(\rho c p)_{f}}\right]+\phi_{1}\frac{(\rho c p)_{1}}{(\rho c p)_{f}}}\left[1+\frac{4R_{a}}{3}\right]y_{5}'=$$

$$(22)$$

$$\left(\frac{\frac{2}{m+1}}{P_r y_2 y_4} + \frac{\frac{2}{m+1}}{m+1} P_r S_t y_2\right) - P_r y_1 y_5 - P_r N_b y_5 y_7 - P_r N_t y_5 y_5 - \frac{2}{m+1} \zeta P_r Exp^{-n\eta}\right)$$

$$q = y_6, \ q' = y_7, \ q'' = y_7',$$
 (23)

$$y_7' = \frac{N_t}{N_h} y_5' - S_{cA} y_1 y_7 + \frac{2}{m+1} S_{cA} \mathcal{R} y_6(\eta) (y_8)^3(\eta),$$
 (24)

$$s = y_8, s' = y_9, s'' = y_9'$$
 (25)

$$\gamma y_9' = \frac{N_t}{N_h} y_5' - S_{cB} y_1 y_9 - \frac{2}{m+1} S_{cB} \mathcal{R} y_6(\eta) (y_8)^3(\eta) = 0,$$
 (26)

Boundary Conditions

$$y_{1} = 0, \ y_{2} = 1, \ y_{4} = 1 - S_{t}, \ y_{7} = \mathcal{J}y_{6}, \ \gamma y_{9} = -\mathcal{J}y_{6}, \ at \ \eta = 0,$$

$$y_{2} \to 0, \ y_{4} \to 0, \ y_{6} \to 1, \ y_{8} \to 0, \ as \ \eta \to \infty$$

$$(27)$$

4. Results and discussion

This section describes the computational findings obtained via the Bvp4c numerical approach. This employed numerical technique is to demonstrate the fundamental physical principles that govern the flow, temperature, and concentration of homogeneous bulk fluid as result of non-dimension parameters and other features are shown in Figs. 2-11. Furthermore, computed numerical outcomes for different controlling parameters against heat gradients is presented in tabular form.

Fig. 2 displays the impact of Gr on velocity profile for St = 0.1. The Grashof number is a dimensionless parameter that illustrates the relationship between buoyancy forces and viscous forces within a fluid flow. An increased

Gr also implies an increase of the buoyancy force within the fluid. As the Gr upsurges, the buoyancy force within the velocity flow also raises. A higher Grashof number indicates that the incoming flow gives the fluid particles a stronger upward force, thus increasing their rate of acceleration in the flow direction. This in turn results to improvement of convective motion within the fluid due to increase in the buoyancy force. As the temperature gradient between the warmer and cooler regions of the fluid widens, the Grashof number will correspondingly rise. This results in a stronger velocity profile. Physically, in a heated fluid, expansion occurs because of temperature differences that affect density. The fluid near the hot surface becomes lighter and rises. As this hot, less dense fluid moves upward, cooler, denser fluid moves in to



fill the space, creating a convection current. This process is driven by buoyancy and is related to

the Grashof number for mass transfer.

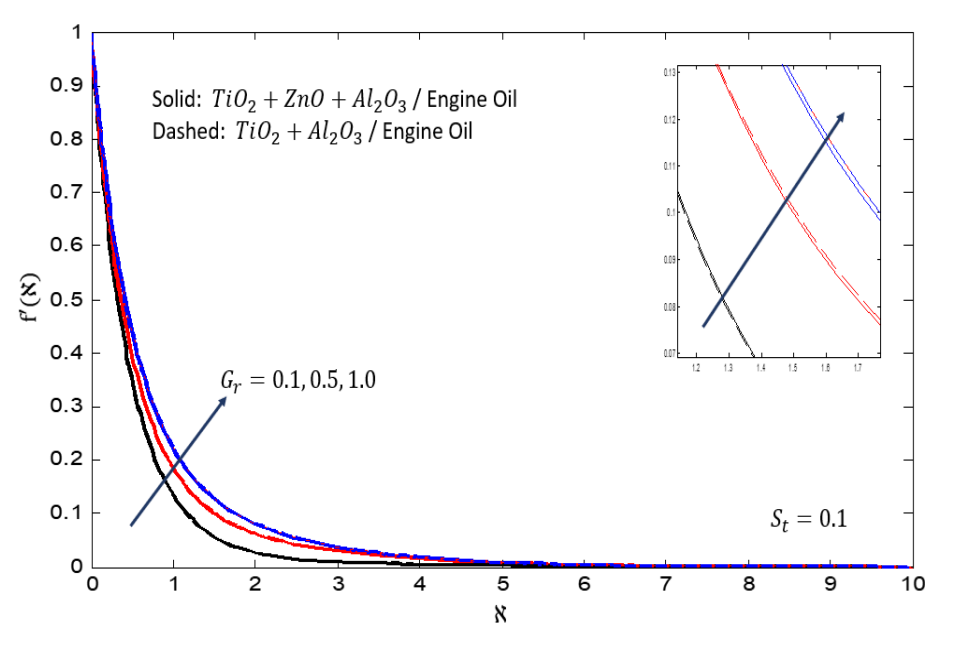


Fig. 2: Effect of G_r on velocity profile when $S_t = 0.1$

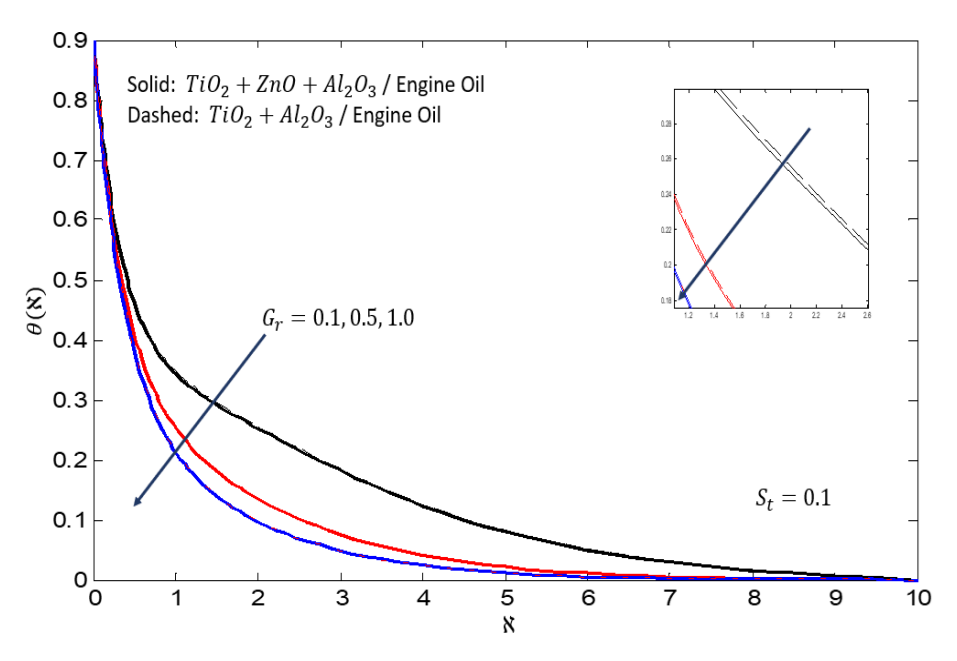


Fig. 3 Effect of Gr on temperature profile when $S_t = 0.1$

Fig 3 reveals the implication of Grashof number Gr on the temperature profile for St = 0.1. As Gr increases there is a corresponding augmentation in the natural convection flow within the fluid. This phenomenon curtails the thermal conduction towards the heated surface, thereby

elevating the temperature gradient in the fluid. Consequently, the temperature gradient within the thermal boundary layer amplifies more significantly as it distances itself from the heated surface. With higher Grashof numbers, the fluid in proximity to the heated surface tends to ascend



more prominently due to buoyancy. This results in a swifter removal of warm fluid from the surface, consequently accelerating the movement of the fluid adjacent to the surface. Consequently, the temperature decreases more swiftly near the heated surface leading to a reduction in the overall temperature distribution in the fluid.

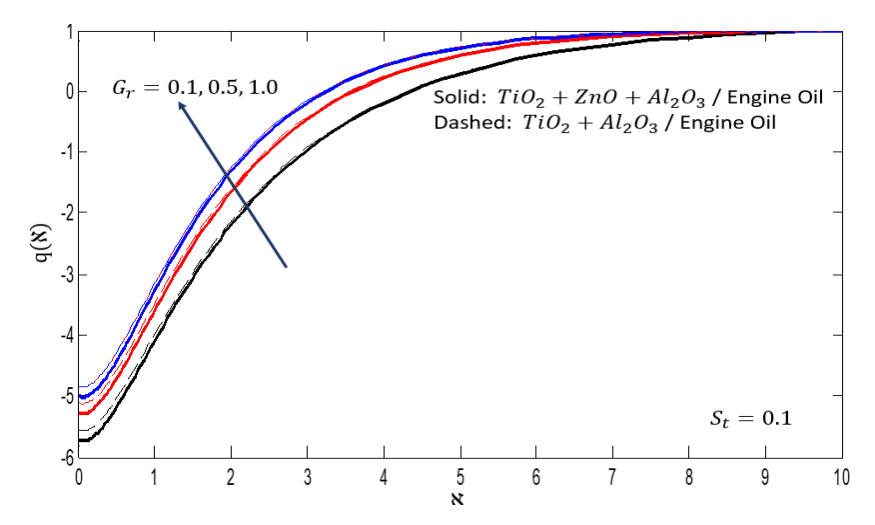


Fig.4 Effect of G_r on concentration of homogeneous bulk fluid profile

Fig 4 shows the outcome of Gr on concentration distribution of homogeneous bulk fluid profile for St=0.1. As the Gr increases on the vertical axis, there is a noticeable augmentation in concentration distribution of the homogeneous bulk fluid. The Grashof number is an important parameter that compares the buoyancy force to the viscous force in the fluid. When Gr increases, buoyancy forces become stronger than viscous forces. This enhanced buoyancy leads to more vigorous natural convection currents, which

improve the diffusion and movement of species within the fluid. As a result, the species concentration in the bulk of the carrier fluid increases. This effect is particularly pronounced when the local density of species is influenced by temperature gradients, as the buoyancy-driven flow aids in transporting species throughout the fluid. Furthermore, the effect of Gr on velocity profile for St=0.9 is display in Fig. 5. It was seen that the impact of Gr on fluid flow when St =0.9.

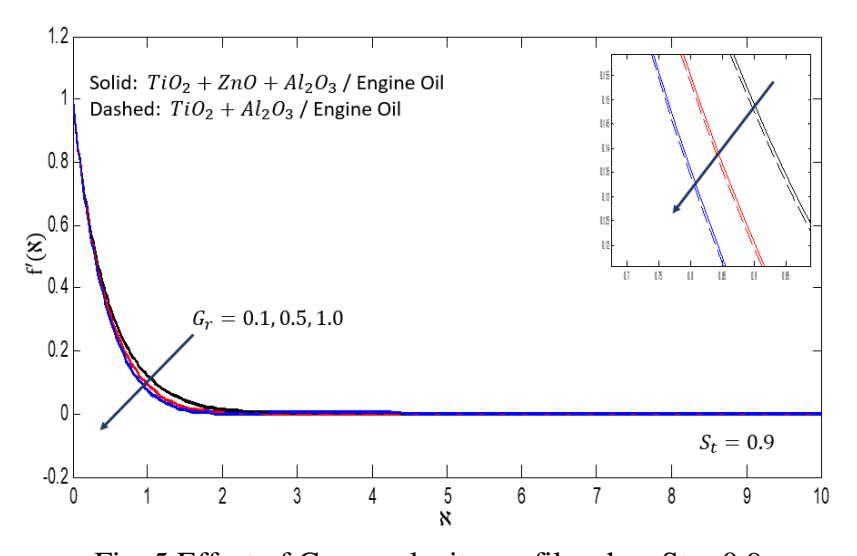


Fig. 5 Effect of Gr on velocity profile when St = 0.9



Fig. 6 illustrates the influence of Ra on the velocity profile at St= 0.1. The introduction of thermal radiation increases the energy within the fluid system, subsequently enhancing the thermal energy of the fluid particles. The rise in thermal energy causes viscosity of the fluid to decline, as viscosity typically decreases with enhanced temperatures particularly in the case of liquids. Therefore, the fluid flows with lesser resistance which in a way increases the velocity of the fluid which is being transferred. Additionally, thermal radiation can cause energy to create a temperature difference in the fluid. This temperature gradient can lead to buoyancy-

driven flow, especially in areas where the fluid is heated and becomes less dense. This buoyancy acts as a force that increases the fluid's velocity, further accelerating its movement. Also, TiO_2 + $ZnO + Al_2O_3$ / Engine Oil is greater than the TiO2 + Al2O3 / Engine Oil. Furthermore, Fig. 7 illustrates how thermal radiation affects the temperature profile. The primary contributing to the rise in temperature is the enhanced absorption of heat from the surface via $TiO_2 + ZnO + Al_2O_3$ Also, Engine Oil is higher than the $TiO_2 + Al_2O_3$ / Engine Oil.

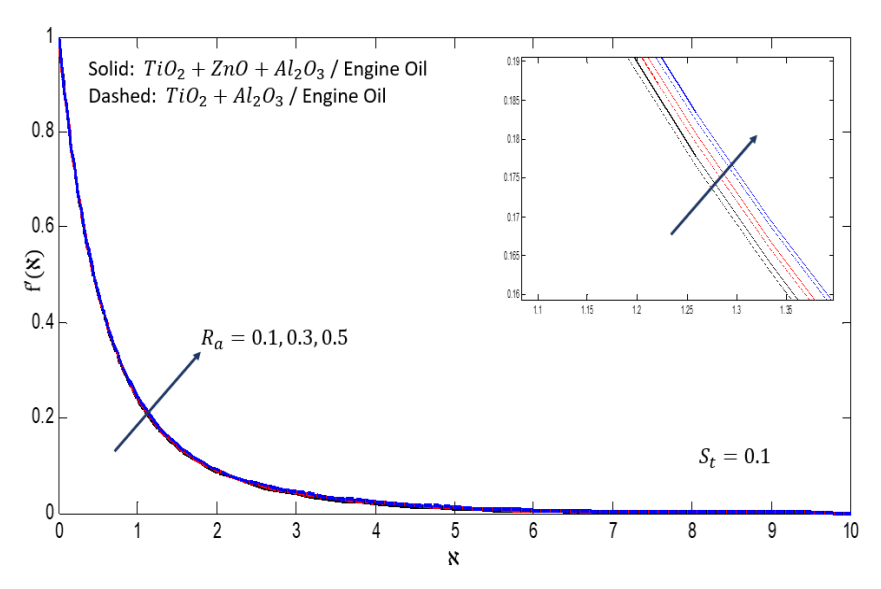


Fig.6 Effect of Ra on velocity profile when St=0.1

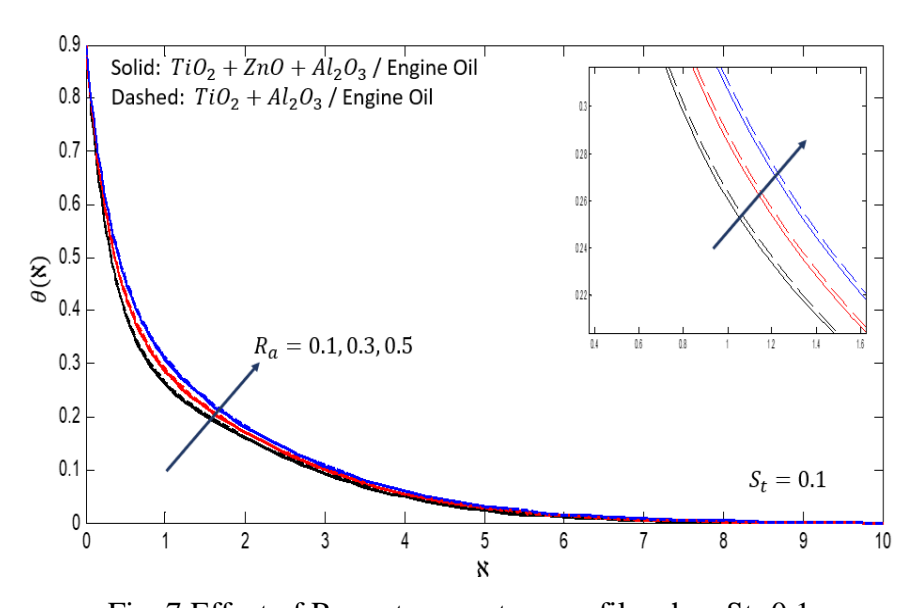


Fig. 7 Effect of Ra on temperature profile when St=0.1



Fig. 8 Effect of Radiation Ra on concentration of homogeneous bulk fluid profile when St= 0.1. However, it was observed that the impact Ra elevate the homogeneous bulk fluid profile. Furthermore, Ra enhances the total heat transfer within the catalyst constituent to the surface of the catalyst. One of the limitations in heterogeneous catalysis, is that the surface temperature of the catalyst exerts significant influence on the reaction kinetic. Incremental values of Ra leads to increase in the surface

temperature, and the rate of catalytic reactions also increase (See Fig. 9). The change in parameter resulting in conservation of thermal radiation that causes an enhancement in the catalytic activity. Catalysts are known to exist at their best performing temperature at which they show the highest level of activity. The factors affecting the efficiency of the catalytic process can be brought to the desired level with the help of thermal radiation that contributes to the increase of the surface temperature.

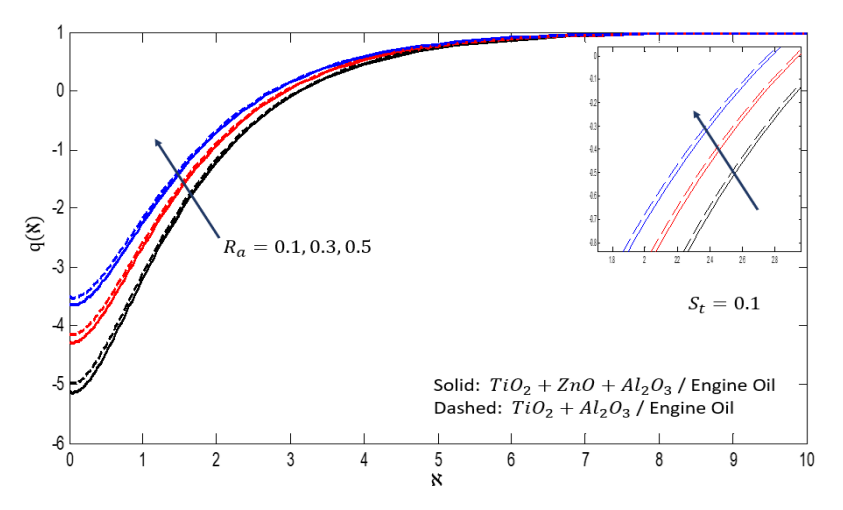


Fig.8 Effect of Ra on concentration of homogeneous bulk fluid profile

When St=0.1

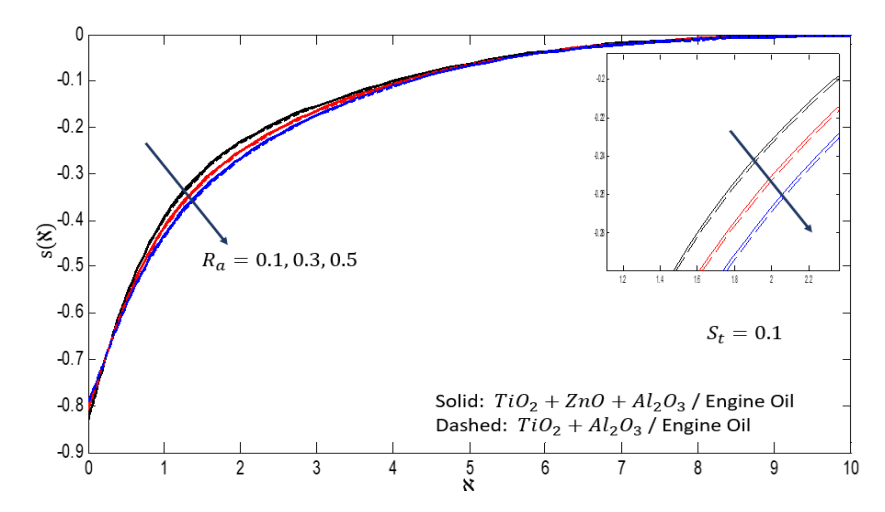


Fig. 9 Effect of Ra on concentration of heterogeneous catalyst at the surface profile when St=0.1

Fig. 8 Effect of Ra on concentration of homogeneous bulk fluid profile when St= 0.1. However, it was observed that the impact Ra elevate the homogeneous bulk fluid profile.

Furthermore, thermal radiation enhances the total heat transfer within the catalyst constituent to the surface of the catalyst. One of the limitations in heterogeneous catalysis, is that the



surface temperature of the catalyst exerts significant influence on the reaction kinetic. With a rise in the thermal radiation the surface temperature increases, and the rate of catalytic reactions also increase (See Fig. 9). The change in parameter resulting in conservation of thermal radiation that causes an enhancement in the

catalytic activity. Catalysts are known to exist at their best performing temperature at which they show the highest level of activity. The factors affecting the efficiency of the catalytic process can be brought to the desired level with the help of thermal radiation that contributes to the increase of the surface temperature.

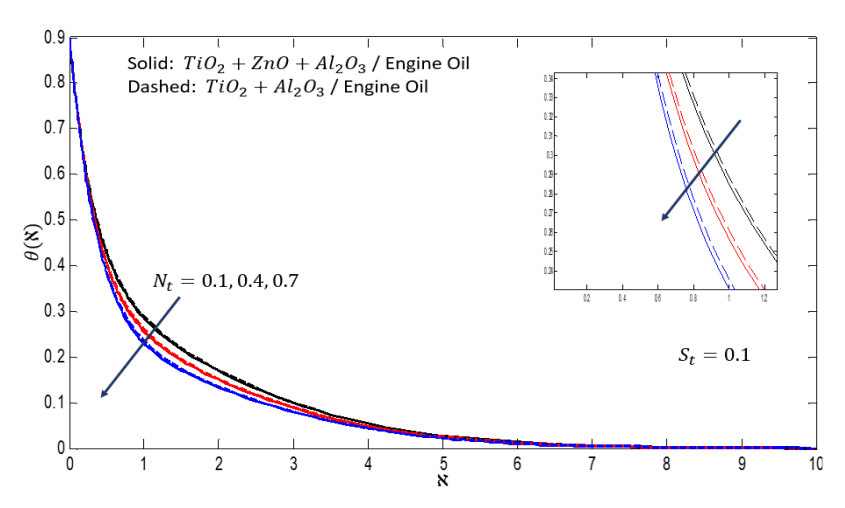


Fig. 10 Effect of Nt on temperature profile when St=0.1

Fig. 10 and Fig. 11 show the impacts of Nt and Nb on temperature profile. An escalation in the quantity of Nb leads to an improvement in its temperature profile, whereas a rise in Nt causes a decrease in the temperature profile. As the Nb improves, the fluid temperature of the fluid system improves. This indicates that as Nb

upsurges the particle mobility intensifications, and the random movement of the nanoparticles upsurges thus the energy distribution in the fluid becomes more distributed which raises the fluid temperature. On the other hand, an increase in the Nt reduce the fluid temperature.

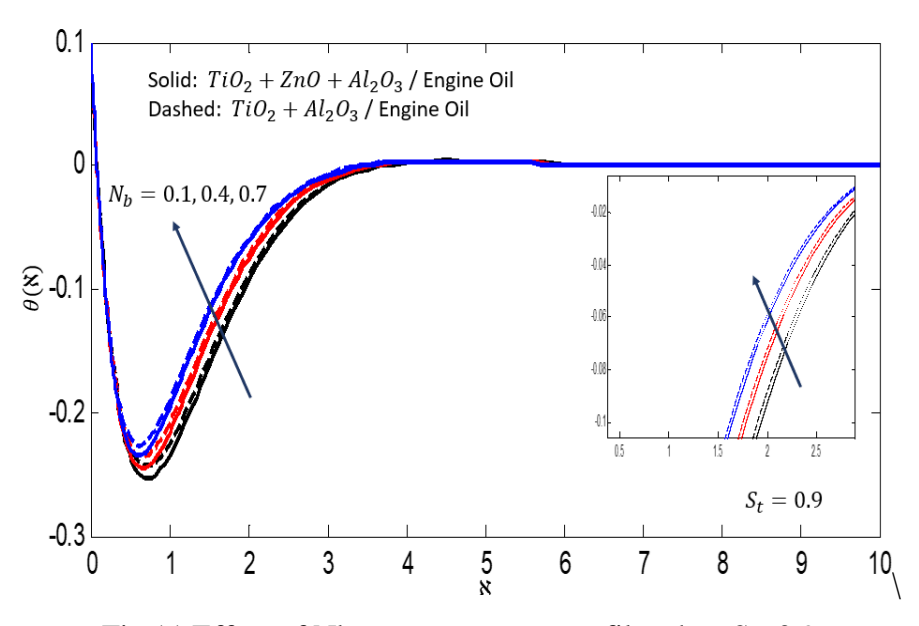


Fig.11 Effect of Nb on temperature profile when St=0.9



Table 2: The numerical values of varied parameters for $Nu_x^{-1/2}$

Values	$Nu_x^{1/2}$
0.1	-0.364011
0.2	-0.905159
0.3	-1.448028
0.4	-1.990012
0.3	-0.377683
0.5	-0.387415
0.7	-0.393005
0.9	-0.394433
0.4	-0.332294
0.6	-0.280014
0.8	-0.232747
0.1	-0.302326
0.2	-0.360396
0.3	-0.352011
0.4	-0.340612
	0.1 0.2 0.3 0.4 0.3 0.5 0.7 0.9 0.4 0.6 0.8 0.1 0.2 0.3

Table 2 displays the numerical values of chosen parameters for $u_x^{-\frac{1}{2}}$. As Ntupsurges from 0.1 to 0.4, the value declines from -0.364 to -1.990. When Strises from 0.3 to 0.9, the value declines slightly from -0.378 to -0.394. Similarly, growing value of Ra from 0.4 to 0.8 results in a decrease in the value, from -0.332 to -0.233, with this decrease being more substantial than St. Growing Ps from 0.1 to 0.2 leads to a lessening in the value, but further increases in Ps to 0.3 and 0.4 cause the value to rise slightly.

5. Conclusion

In summary, we examined the thermal stability and sustainability impact of TiO_2 , ZnO, Al_2O_3 in an engine oil based Casson fluid of a solar photovoltaic system with homogeneous-heterogeneous chemical reaction within a stratified nonlinear surface. The present study is inspired by improving the thermal radiation

phenomena afterward employed in solar photovoltaic system for numerous uses. The main findings of the present investigation are outlined as follows:

- The $Nu_x^{-\frac{1}{2}}$ declines with the higher value of Nt, St, Ra, Ps.
- The velocity profile is larger for Grashof number when St =0.1 in the boundary layer.
- Velocity and temperature profile of the system is detected to upsurge with increase in material parameter.
- The homogeneous bulk fluid increase with the growing upshot of the Grashof number when St = 0.1.

An increase in Nb improve the fluid temperature, while Nt reduces when St= 0.9



REFERENCES

- [1] T. Z. Ang, M. Salem, M. Kamarol, H. S. Das, M. A. Nazari, and N. Prabaharan, "A comprehensive study of renewable energy sources: Classifications, challenges and suggestions," *Energy Strategy Rev.*, vol. 43, p. 100939, 2022.
- [2] L. Hernández-Callejo, S. Gallardo-Saavedra, and V. Alonso-Gómez, "A review of photovoltaic systems: Design, operation and maintenance," *Sol. Energy*, vol. 188, pp. 426–440, 2019.
- [3] L. Thapa, H. Durrast, S. Gyawali, and K. Techato, "A review on solar energy photovoltaic (PV) system potential and challenges in Nepal," SSRN 4282393, 2022.
- [4] Y. Elomari, M. Norouzi, M. Marín-Genescà, A. Fernández, and D. Boer, "Integration of solar photovoltaic systems into power networks: A scientific evolution analysis," *Sustainability*, vol. 14, no. 15, p. 9249, 2022.
- [5] M. A. de Brito, L. P. Sampaio, L. G. Junior, and C. A. Canesin, "Research on photovoltaics: review, trends and perspectives," in *Proc. XI Brazilian Power Electron. Conf.*, 2011, pp. 531–537.
- [6] N. A. Shah, "Stagnation point on the micropolar bioconvection nanofluid flow over inclined Riga plate: Keller box analysis," *Phys. Fluids*, vol. 37, no. 1, 2025.
- [7] Ramesh, G. K., Madhukesh, J. K., Das, R., Shah, N. A., & Yook, S. J. (2025). Thermodynamic activity of a ternary nanofluid flow passing through a permeable slipped surface with heat source and sink. Waves in Random and Complex Media, 35(2), 3499-3519.
- [8] A. Rauf, Faisal, N. A. Shah, and T. Botmart, "Hall current and morphological effects on MHD micropolar non-Newtonian tri-hybrid nanofluid flow between two parallel surfaces," *Sci. Rep.*, vol. 12, no. 1, p. 16608, 2022.
- [9] K. Ramesh, K. K. Asogwa, T. Oreyeni, M. G. Reddy, and A. Verma, "EMHD radiative titanium oxide-iron oxide/ethylene glycol hybrid nanofluid flow over an exponentially stretching sheet," *Biomass Convers. Biorefin.*, vol. 14, no. 16, pp. 18887–18896, 2024.

- [10] O. K. Koriko, N. A. Shah, S. Saleem, J. D. Chung, A. J. Omowaye, and T. Oreyeni, "Exploration of bioconvection flow of MHD thixotropic nanofluid past a vertical surface coexisting with both nanoparticles and gyrotactic microorganisms," *Sci. Rep.*, vol. 11, no. 1, p. 16627, 2021.
- [11] N. A. Shah, O. Tosin, R. Shah, B. Salah, and J. D. Chung, "Brownian motion and thermophoretic diffusion effects on the dynamics of MHD upper convected Maxwell nanofluid flow past a vertical surface," *Phys. Scr.*, vol. 96, no. 12, p. 125722, 2021.
- [12] Q. Raza, S. Li, X. Wang, B. Ali, and N. A. Shah, "Finite element analysis of morphological effects and nanolayer thermal conductivity in Boger nanofluids under thermal radiation," *Chaos, Solitons Fractals*, vol. 199, p. 116644, 2025.
- [13] M. J. Babu, Y. S. Rao, A. S. Kumar, C. S. K. Raju, S. A. Shehzad, T. Ambreen, and N. A. Shah, "Squeezed flow of polyethylene glycol and water based hybrid nanofluid over a magnetized sensor surface: a statistical approach," *Int. Commun. Heat Mass Transfer*, vol. 135, p. 106136, 2022.
- [14] K. K. Asogwa, B. S. Goud, N. A. Shah, and S. J. Yook, "Rheology of electromagnetohydrodynamic tangent hyperbolic nanofluid over a stretching Riga surface featuring Dufour effect and activation energy," *Sci. Rep.*, vol. 12, no. 1, p. 14602, 2022.
- [15] Rasool, G., Shah, N. A., El-Zahar, E. R., & Wakif, A. (2025). Numerical investigation of EMHD nanofluid flows over a convectively heated riga pattern positioned horizontally in a Darcy-Forchheimer porous medium: Application of passive control strategy and generalized transfer laws. Waves in Random and Complex Media, 35(3), 6039-6058.
- [16] Rauf, A., Faisal, Hussain, F., & Shah, N. A. (2025). A numerical study of Carreau—Yasuda tri-hybrid nanofluid over a convective heated surface near a stagnation point. Journal of Thermal Analysis and Calorimetry, 1-12.
- [17] Yu, Liping, Yijie Li, Venkatesh Puneeth, Sami Znaidia, Nehad Ali Shah, Sarpabhushana



- Manjunatha, Muhammad Shoaib Anwar, and Muhammad Riaz Khan. "Heat transfer optimisation through viscous ternary nanofluid flow over a stretching/shrinking thin needle." Numerical Heat Transfer, Part A: Applications 86, no. 3 (2025): 518-532.
- [18] M. D. Kumar, G. Dharmaiah, S. J. Yook, C. S. K. Raju, and N. A. Shah, "Deep learning approach for predicting heat transfer in water-based hybrid nanofluid thin film flow and optimization via response surface methodology," *Case Stud. Therm. Eng.*, vol. 68, p. 105930, 2025.
- [19] Ramasekhar, Gunisetty, A. Divya, P. D. Selvi, Ramaiah Narayanagari, R. Chandra Sekhar Reddy, Shaik Jakeer, Seethi Reddy Reddisekhar Reddy, Sangapatnam Suneetha, Nehad Ali Shah, and Shams Forruque Ahmed. "Exploring the role of Casson hybrid nanofluid flow through a stretching cylinder with a significant impact of heat source/sink: A computational analysis." AIP Advances 15, no. 3 (2025).
- [20] M. D. Kumar, C. S. K. Raju, N. A. Shah, S. J. Yook, and D. Gurram, "Support vector machine learning classification of heat transfer rate in tri-hybrid nanofluid over a 3D stretching surface with suction effects for water at 10 °C and 50 °C," *Alex. Eng. J.*, vol. 118, pp. 556–578, 2025.
- [21] M. Yaseen, S. K. Rawat, N. A. Shah, M. Kumar, and S. M. Eldin, "Ternary hybrid nanofluid flow containing gyrotactic microorganisms over three different geometries with Cattaneo-Christov model," *Mathematics*, vol. 20, p. 1237, 2023.
- [22] Vinodkumar Reddy, M., Nath, J. M., Das, T. K., Ali, F., & Shah, N. A. (2025). Mixed convection flow on the Hall current effect of Ree-Eyring nanomaterial with gyrotactic microorganism and heat radiation flow. Journal of Thermal Analysis and Calorimetry, 1-21.
- [23] Yahya, A. U., Salamat, N., Abdal, S., & Shah, N. A. (2025). Modified Buongiorno model for MHD micropolar and Casson hybrid nanofluid transportation with nonlinear thermal radiation through porous channel. Journal of Thermal Analysis and Calorimetry, 1-17.

- [24] Ramasekhar, G., & Shah, N. A. (2025). Theoretical investigation of the Casson hybrid nanofluid flow through a stretching surface with thermal radiation: a biomedical application. The European Physical Journal Plus, 140(2), 1-11.
- [25] Li, G., Abdal, S., Zhang, B., Shah, N. A., & Fatima, Z. (2025). Bioconvection for Riga wedge flow of tangent hyperbolic nanofluids in the presence of activation energy and mass suction. Journal of Thermal Analysis and Calorimetry, 1-17.
- [26] T. Oreyeni, A. M. Obalalu, A. O. Popoola, E. O. Omole, B. Souayeh, K. P. Ajewole, and O. J. Akinremi, "Quartic autocatalytic reaction in a bioconvective flow of a stratified EHMD Casson fluid conveying nanoparticles over a surface with variable thickness: Legendre based collocation approach," in *Proc. Int. Conf. Sci., Eng. Bus. Driving Sustainable Develop. Goals* (SEB4SDG), Apr. 2024, pp. 1–14.
- [27] B. M. Tamilzharasan, S. Karthikeyan, M. K. Kaabar, M. Yavuz, and F. Özköse, "Magneto mixed convection of Williamson nanofluid flow through a double stratified porous medium in attendance of activation energy," *Math. Comput. Appl.*, vol. 27, no. 3, p. 46, 2022.
- [28] K. Jagan and S. Sivasankaran, "Soret & Dufour and triple stratification effect on MHD flow with velocity slip towards a stretching cylinder," *Math. Comput. Appl.*, vol. 27, no. 2, p. 25, 2022.
- [29] S. Rehman, A. Anjum, M. Farooq, and M. Y. Malik, "Melting heat phenomenon in thermally stratified fluid reservoirs (Powell-Eyring fluid) with joule heating," *Int. Commun. Heat Mass Transfer*, vol. 137, p. 106196, 2022.
- [30] T. Oreyeni, K. Ramesh, M. K. Nayak, and P. A. Oladele, "Triple stratification impacts on an inclined hydromagnetic bioconvective flow of micropolar nanofluid with exponential spacebased heat generation," *Waves Random Complex Media*, pp. 1–23, 2022.
- [31] M. Fayz-Al-Asad, T. Oreyeni, M. Yavuz, and P. O. Olanrewaju, "Analytic simulation of MHD boundary layer flow of a chemically reacting upper-convected Maxwell fluid past a vertical surface subjected to double



- stratifications with variable properties," *Eur. Phys. J. Plus*, vol. 137, no. 7, p. 813, 2022.
- [32] W. A. Khan, N. Anjum, M. Waqas, S. Z. Abbas, M. Irfan, and T. Muhammad, "Impact of stratification phenomena on a nonlinear radiative flow of Sutterby nanofluid," *J. Mater. Res. Technol.*, vol. 15, pp. 306–314, 2021.
- [33] K. Guedri, P. Singh, F. Riaz, A. Inayat, N. A. Shah, B. M. Fadhl, and A. Arsalanloo, "Solidification acceleration of phase change material in a horizontal latent heat thermal energy storage system by using spiral fins," *Case Stud. Therm. Eng.*, vol. 48, p. 103157, 2023.
- [34] A. S. Dogonchi, N. S. Bondareva, M. A. Sheremet, S. El-Sapa, A. J. Chamkha, and N. A. Shah, "Entropy generation and heat transfer performance analysis of a non-Newtonian NEPCM in an inclined chamber with complicated heater inside," *J. Energy Storage*, vol. 72, p. 108745, 2023.
- [35] P. Priyadharshini, M. V. Archana, N. A. Ahammad, C. S. Raju, S. J. Yook, and N. A. Shah, "Gradient descent machine learning regression for MHD flow: Metallurgy process," *Int. Commun. Heat Mass Transfer*, vol. 138, p. 106307, 2022.
- [36] C. S. Sravanthi, F. Mabood, S. G. Nabi, and S. A. Shehzad, "Heterogeneous and homogeneous reactive flow of magnetite-water nanofluid over a magnetized moving plate," *Propuls. Power Res.*, vol. 11, no. 2, pp. 265–275, 2022.
- [37] F. Alzahrani, R. P. Gowda, R. N. Kumar, and M. I. Khan, "Dynamics of thermosolutal Marangoni convection and nanoparticle aggregation effects on Oldroyd-B nanofluid past a porous boundary with homogeneous-heterogeneous catalytic reactions," *J. Indian Chem. Soc.*, vol. 99, no. 6, p. 100458, 2022.
- [38] G. Sarojamma, R. Vijaya Lakshmi, P. V. Satya Narayana, and I. L. Animasaun, "Exploration of the significance of autocatalytic chemical reaction and Cattaneo-Christov heat flux on the dynamics of a micropolar fluid," *J. Appl. Comput. Mech.*, vol. 6, no. 1, pp. 77–89, 2020.

- [39] I. L. Animasaun, B. Mahanthesh, G. Sarojamma, and J. S. Damisa, "Significance of thickness of paraboloid of revolution and buoyancy forces on the dynamics of Eyring—Powell fluid subject to equal diffusivity kind of quartic autocatalysis," *Physica A*, vol. 549, p. 124047, 2020.
- [40] T. Hayat, Z. Hussain, T. Muhammad, and A. Alsaedi, "Effects of homogeneous and heterogeneous reactions in flow of nanofluids over a nonlinear stretching surface with variable surface thickness," *J. Mol. Liq.*, vol. 221, pp. 1121–1127, 2016.
- [41] Q. Zhao, H. Xu, and L. Tao, "Homogeneous-heterogeneous reactions in boundary-layer flow of a nanofluid near the forward stagnation point of a cylinder," *J. Heat Transf.*, vol. 139, no. 3, 2016.
- [42] N. A. Shah, O. K. Koriko, K. Ramesh, and T. Oreyeni, "Rheology of bioconvective stratified Eyring-Powell nanofluid over a surface with variable thickness and homogeneous-heterogeneous reactions," *Biomass Convers. Biorefin.*, vol. 14, no. 17, pp. 20823–20839, 2024.
- [43] N. A. Shah, A. O. Popoola, T. Oreyeni, E. Omokhuale, and M. M. Altine, "A modelling of bioconvective flow existing with tiny particles and quartic autocatalysis reaction across stratified upper horizontal surface of a paraboloid of revolution," *Math. Model. Numer. Simul. Appl.*, vol. 3, no. 1, pp. 74–100, 2023.
- [44] O. K. Koriko, A. J. Omowaye, N. Sandeep, and I. L. Animasaun, "Analysis of boundary layer formed on an upper horizontal surface of a paraboloid of revolution within nanofluid flow in the presence of thermophoresis and Brownian motion of 29 nm CuO," *Int. J. Mech. Sci.*, vol. 124, pp. 22–36, 2017.
- [45] R. Gandhi, B. K. Sharma, N. K. Mishra, and Q. M. Al-Mdallal, "Computer simulations of EMHD Casson nanofluid flow of blood through an irregular stenotic permeable artery: application of Koo-Kleinstreuer-Li correlations," *Nanomaterials*, vol. 13, no. 4, p. 652, 2023.
- [46] T. Oreyeni, N. A. Shah, A. O. Popoola, E.



R. Elzahar, and S. J. Yook, "The significance of exponential space-based heat generation and variable thermophysical properties on the

dynamics of Casson fluid over a stratified surface with non-uniform thickness," *Waves Random Complex Media*, pp. 1–19, 2022.

